Publication Year	2018
Acceptance in OA	2020-09-23T10:29:25Z
Title	KIC 7599132: an ellipsoidal variable in a close SB1 system
Authors	CATANZARO, Giovanni, FRASCA, Antonio, Giarrusso, M., RIPEPI, Vincenzo, LEONE, FRANCESCO, Tognelli, E., MUNARI, MATTEO, SCUDERI, Salvatore
Publisher's version (DOI)	10.1093/mnras/sty722
Handle	http://hdl.handle.net/20.500.12386/27469
Journal	MONTHLY NOTICES OF THE ROYAL ASTRONOMICAL SOCIETY
Volume	477

Monthly Notices of the ROYAL ASTRONOMICAL SOCIETY

MNRAS **477,** 2020–2029 (2018) doi:10.1093/mnras/sty722
Advance Access publication 2018 March 17

KIC 7599132: an ellipsoidal variable in a close SB1 system

G. Catanzaro,[1]★ A. Frasca,[1] M. Giarrusso,[2] V. Ripepi,[3] F. Leone,[1,4] E. Tognelli,[5,6] M. Munari[1] and S. Scuderi[1]

[1]*INAF – Osservatorio Astrofisico di Catania, Via S.Sofia 78, I-95123, Catania, Italy*
[2]*INFN, Laboratori Nazionali del Sud, Via S. Soa 62, I-95123 Catania, Italy*
[3]*INAF – Osservatorio Astronomico di Capodimonte, Via Moiariello 16, I-80131 Napoli, Italy*
[4]*Universitá degli studi di Catania, Via S.Sofia 78, I-95123, Catania, Italy*
[5]*Osservatorio Astronomico di Teramo, via M. Maggini, I-64100, Teramo, Italy*
[6]*INFN, Sezione di Pisa, Largo Bruno Pontecorvo 3, I-56127, Pisa, Italy*

Accepted 2018 March 14. Received 2018 March 14; in original form 2017 July 11

ABSTRACT

In this paper, we present a spectroscopic and photometric analysis of the suspected ellipsoidal variable star KIC 7599132. New spectroscopic observations have been obtained with Catania Astrophysical Observatory Spectropolarimeter. From the fit of Hα and Hβ, we determined the effective temperature and gravity of the primary component, $T_{\rm eff} = 10200 \pm 150$ K and $\log g = 4.1 \pm 0.1$, while from a number of metal lines, we derive the rotational velocity, $v_{\rm e}\sin i = 60 \pm 2$ km s^{-1}. We found almost solar abundances with the exception of silicon (0.50 dex) overabundance. A Bayesian analysis, based on the comparison between observational data and theoretical predictions of PROSECCO evolutionary models, allows us to estimate the mass and the age of the primary. We obtained $M_1 = 2.4 \pm 0.2$ M$_\odot$ and $\tau_{\rm s} = 3.8^{+0.9}_{-0.7}$ Myr. A new model for the system was obtained combining *Kepler* photometric time series (Q0–Q17) and our radial velocities by using the code PHOEBE. As a result, the system appears to be a detached binary system with a mass ratio $q = 0.30 \pm 0.01$, a semimajor axis $a = 7.3 \pm 0.1$ R$_\odot$ and an inclination angle $i = 35^\circ \pm 2^\circ$. This modelling allowed us to derive: $M_2 = 0.7 \pm 0.1$ M$_\odot$, $R_1 = 3.0 \pm 0.2$ R$_\odot$, and $R_2 = 1.5 \pm 0.2$ R$_\odot$. Numerical simulations show that if the secondary star had been hotter than 4000 K, we would have observed its spectral features in our spectra.

Key words: stars: abundances – binaries: close – binaries: spectroscopic – stars: evolution – stars: fundamental parameters – stars: individual: HD 180757.

1 INTRODUCTION

The *Kepler* four-year space mission and its *K2* extension provide photometric time series with unprecedented precision. Given the relevance of these data on the studies about stellar pulsations, the introduction of large data bases, as homogeneous as possible, collecting important astrophysical parameters such as temperature, gravity, and metallicity becomes necessary. The LAMOST-*Kepler* project, based on LAMOST spectroscopy of *Kepler* targets, aims at providing the atmospheric parameters and other basic data for thousands of stars, which fall in the field of view of the *Kepler* telescope (De Cat et al. 2015).

In the framework of LAMOST-*Kepler* project, a recent paper by Frasca et al. (2016) focuses on the determination of activity indicators, atmospheric parameters, radial, and rotational velocities with the code ROTFIT, developed by Frasca et al. (2003, 2006), for a sample of about 60 000 stars of the *Kepler* field that were observed from 2011 to 2014. In that paper, a comparison with data from the literature for a few hundred targets allowed the authors to assess the accuracy of the derived parameters and to identify objects with discrepant values. Regarding the radial velocity (RV), only one star, namely KIC 7599132 (= HD 180757), observed by LAMOST for two times, has been found discrepant from precedent results (Catanzaro et al. 2010).

KIC 7599132 was inserted in a list of possible Slowly Pulsating B-type stars by Lehmann et al. (2011). These authors performed a local thermodynamic equilibrium spectral synthesis of a high-resolution spectrum obtaining the following atmospheric parameters: $T_{\rm eff} = 11090^{+100}_{-400}$ K, $\log g = 4.08 \pm 0.06$, $v_{\rm e}\sin i = 63^{+5}_{-4}$ km s^{-1}, $\xi = 1.6^{+0.5}_{-0.6}$ km s^{-1}, and metallicity [M/H] $= 0.06 \pm 0.10$.

Moreover, *Kepler* photometry of KIC 7599132 from quarters Q0 to Q4 was first presented by Balona et al. (2011) in their study of 48 B-type stars in which they discussed the types of variability that might be found among B stars. In that paper, the authors suggested that KIC 7599132 could be a member of a close binary system.

★ E-mail: gca@oact.inaf.it

© 2018 The Author(s)
Published by Oxford University Press on behalf of the Royal Astronomical Society

Downloaded from https://academic.oup.com/mnras/article-abstract/477/2/2020/4942279 by guest on 26 February 2020

This star is included in the catalogue by McNamara, Jackiewicz & McKeever (2012), where it is classified as a rotationally variable star or close binary. Complete *Kepler* photometry (quarters 0–17) has been taken into account in Balona et al. (2015), who found a single harmonic series in the periodogram, with the fundamental frequency corresponding to $P = 1.303685 \pm 0.000003$ d. They suggested that this object is probably an ellipsoidal variable (ELL) in a close binary system, but they could not confirm their hypothesis without time-resolved spectroscopy.

The ELL are close binaries whose components are distorted by their mutual gravitation but whose orbital inclinations as seen from Earth are too small to show eclipses. A general characteristic of their light curve (LC) is a large difference in depths of minima indicating component of quite different surface brightness. The light variations are a combination of three effects: tidal distortion, reflection, and beaming. Beaming in particular is induced by the stellar radial motion which results in an increase (decrease) in brightness when the star is approaching (receding from) the observer. As shown by Zucker, Mazeh & Alexander (2007) beaming contribution becomes dominant with respect to ellipsoidal and reflection effects for orbital periods of the order of 10 d or longer, while it is not important for periods of the order of 1 d.

Thus, with the purpose to investigate on the actual nature of KIC 7599132, we decided to insert this star in our ongoing campaign carried out with Catania Astrophysical Observatory Spectropolarimeter (CAOS) aimed at a spectroscopic monitoring of newly discovered binary system (see e.g. Catanzaro et al. 2016).

In the following sections, we present the combined analysis of the *Kepler* photometry and ground-based spectroscopy, which includes determination of atmospheric properties of the primary star (Sections 3–5), RV (Section 6.2), and LC analysis (Sections 6.1 AND 6.3). Finally (Section 7), we speculated on the characteristic of the unseen secondary component.

2 OBSERVATIONS AND DATA REDUCTION

Time-resolved spectroscopy was carried out with the CAOS, which is a fibre fed, high-resolution, cross-dispersed echelle spectrograph (Catanzaro et al. 2015; Leone et al. 2016) installed at the Cassegrain focus of the 91 cm telescope of the *'M. G. Fracastoro'* observing station of the Catania Astrophysical Observatory (Mt. Etna, Italy). In total, 22 spectra were obtained between 2015 and 2017 with exposure times ranging from 1200 to 1800 s; the signal-to-noise ratio (S/N) was at least 50 in the continuum λλ 4300–7000 Å wavelength range, with a resolution of $R = 45\,000$, as measured from ThAr and telluric lines.

The reduction of data, which included subtraction of the bias frame, trimming, correcting for the flat-field and the scattered light, extraction of the orders, and wavelength calibration, was done using the NOAO/IRAF package.[1]

The IRAF task *rvcorrect* was used to determine the heliocentric velocity and to correct the spectra for the Earth's motion.

Considering the S/N of our spectra, we did not find any evidence of spectral lines belonging to the secondary component, at least at a level of 3 per cent of the continuum, thus we classified the system as SB1.

[1] IRAF is distributed by the National Optical Astronomy Observatory (NOAO), which is operated by the Association of Universities for Research in Astronomy, Inc.

Table 1. Heliocentric Julian Date and measured RVs for KIC 7599132.

	HJD (2400000.0 +)	RV (km s^{-1})
CAOS	57269.4143	26.1 ± 3.50
	57271.4429	−58.7 ± 8.12
	57288.3955	−56.1 ± 5.3
	57290.3544	20.3 ± 2.5
	57307.3260	22.5 ± 5.7
	57308.3023	−7.7 ± 2.7
	57309.3396	−57.1 ± 3.4
	57311.2706	25.1 ± 3.5
	57331.3475	−64.6 ± 6.1
	57332.3502	−16.8 ± 4.6
	57336.3144	−34.8 ± 11.7
	57337.3477	16.4 ± 8.0
	57338.3250	−6.8 ± 3.2
	57339.2278	−68.0 ± 3.9
	57340.2174	−30.3 ± 5.8
	57567.5241	−51.6 ± 3.3
	57574.5030	25.9 ± 4.8
	57581.5858	−55.8 ± 6.0
	57610.4773	−52.8 ± 3.1
	57611.4952	−45.6 ± 3.8
	57920.5542	−58.3 ± 2.6
	57934.5578	−0.3 ± 3.7
FRESCO	54308.3540	−57.2 ± 1.8
LAMOST	56432.2612	11.6 ± 17.9
	56570.0049	−51.5 ± 18.9

The RVs reported in Table 1 have been measured by cross-correlating each observed spectrum with a synthetic one computed with the parameters derived in Section 4. The cross-correlation has been calculated by means of the IRAF task *fxcor* excluding Balmer lines as well intervals with telluric lines. We also collected RVs for KIC 7599132 with two further instruments: FRESCO (Catanzaro et al. 2010) and LAMOST (see Frasca et al. 2016, for details).

3 SPECTRAL ENERGY DISTRIBUTIONS

As a first step towards solving this system, we estimated stellar parameters by comparing the observed spectral energy distribution (SED) with synthetic spectra. To this aim, we adopted the VOSA tool (Bayo et al. 2008). The first step was to collect the photometric data by means of the VOSA package. The mean sources of photometry were the *TychoII* (Høg et al. 2000), 2MASS (Skrutskie et al. 2006), *WISE* (Wright et al. 2010) catalogues, complemented with Strömgren (Paunzen 2015), Sloan (Brown et al. 2011), and *GALEX* (*Galaxy Evolution Explorer*)[2] photometry. The second step consisted in estimating the interstellar extinction in magnitude defined as $A_V = R_V \cdot E(B-v)$, where $E(B-v) = 0.201$ has been derived by means of $(B-v)_0 = -0.137$ (Reinhold & Gizon 2015) and the observed $(B-v) = 0.064$ (ESA 1997; Luo et al. 2015). R_V has been fixed equal to 3.1. The observed SED is shown as filled circles in Fig. 1. For the dereddening, VOSA makes use of the extinction law by Fitzpatrick (1999), improved by Indebetouw et al. (2005) for what concerns the infrared spectral range.

Finally, VOSA performed a least-squares fit to this SED by using a grid of ATLAS9 Kurucz ODFNEW/NOVER models (Castelli, Gratton & Kurucz 1997) to obtain a first estimate of

[2] http://galex.stsci.edu/GR6/

Downloaded from https://academic.oup.com/mnras/article-abstract/477/2/2020/4942279 by guest on 26 February 2020

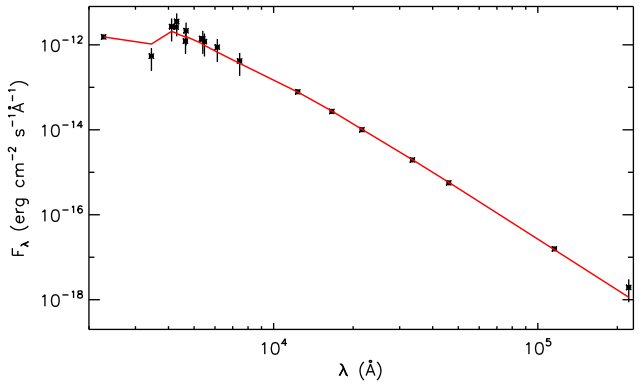

Figure 1. Observed SED for KIC 7599132 as collected by VOSA (dots). The best-fitting Kurucz synthetic spectrum ($T_{\rm eff} = 10250$ K and $\log g = 4.00$) is overplotted with a continuous red line.

temperature and gravity. For this fit, we choose to keep the metallicity fixed to the solar one, since a very preliminary analysis of our spectra does not give any sign of peculiar abundances. The result of this fitting is shown in Fig. 1, where the observed SED is reproduced with the best model computed with $T_{\rm eff} = 10250 \pm 125$ K and $\log g = 4.00 \pm 0.25$.

4 SPECTRAL SYNTHESIS

In A-type stars, Balmer line profiles are sensitive to both effective temperature and surface gravity (e.g. Catanzaro, Leone & Dall 2004, and reference therein).

For the following analysis, we used the spectrum obtained by averaging all the spectra acquired with CAOS corrected for any RV difference. The final spectrum has an S/N of ≈150.

The approach we used in this paper was to minimize the difference between observed and synthetic Hα and Hβ profiles. As goodness-of-fit test we used the parameter:

$$\chi^2 = \frac{1}{N} \sum \left(\frac{I_{\rm obs} - I_{\rm th}}{\delta I_{\rm obs}} \right)^2$$

where N is the total number of points, $I_{\rm obs}$ and $I_{\rm th}$ are the intensities of the observed and computed profiles, respectively, and $\delta I_{\rm obs}$ is the photon noise.

Atmospheric models obtained with ATLAS9 (Kurucz 1993) use pre-computed line opacities in the form of Opacity Distribution Functions, that are tabulated for multiples of the solar metallicity and for various microturbulent velocities.

As a starting values for $T_{\rm eff}$, we used the value derived in the previous section from the fitting of the SED.

To measure the $v_{\rm e}\sin i$, i.e. the projection of the equatorial rotational velocity along the line of sight, we matched synthetic line profiles of KIC 7599132 from SYNTHE (Kurucz & Avrett 1981) to a number of metal lines in the spectral range between 4460 and 4600 Å. The best fit was obtained for $v_{\rm e}\sin i = 60 \pm 2$ km s^{-1}. This value is in agreement with $v_{\rm e}\sin i = 63^{+5}_{-4}$ km s^{-1} reported by Lehmann et al. (2011).

The fitting of Hα and Hβ profiles were generated in three steps: first, we computed the stellar atmosphere models for solar chemical abundances by using the ATLAS9 code, then the stellar spectrum was synthesized using SYNTHE, and finally the instrumental and rotational broadenings were applied. This procedure gave:

$T_{\rm eff} = 10200 \pm 150$ K and $\log g = 4.1 \pm 0.1$.

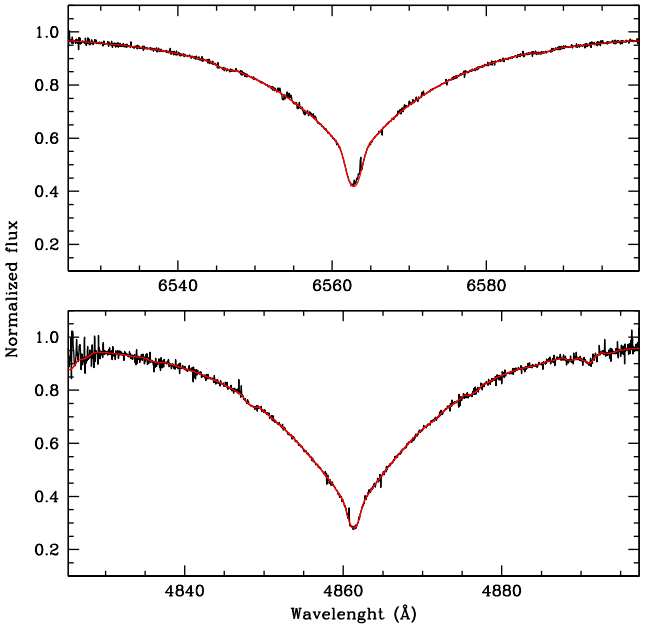

Figure 2. Hα (top panel) and Hβ (bottom panel) for KIC 7599132 with overimposed (red lines) the synthetic spectra computed with the parameters derived in this study.

The result of this fitting procedure is shown in Fig. 2. The obtained $T_{\rm eff}$ and $\log g$ values are in very close agreement with those derived from the SED. However, the value of effective temperature is lower of ≈800 K than those reported in Lehmann et al. (2011), while surface gravity is in close agreement.

The large rotational broadening prevents us from measuring the microturbulent velocity ξ on the metallic lines. Therefore, we adopted the value $\xi = 1.6$ km s^{-1} as determined by Lehmann et al. (2011). To obtain the abundance of individual species, we selected some spectral regions where lines are present and derived the abundances in every interval by performing a χ^2 minimization of the difference between observed and synthetic spectra. The minimization algorithm has been written in IDL[3] language, using the *amoeba* routine. We adopted lists of spectral lines and atomic parameters from Castelli & Hubrig (2004), who updated the parameters listed originally by Kurucz & Bell (1995).

Overabundance of silicon of ≈ 0.5 dex, with respect to the solar values (Asplund et al. 2009), has been derived by fitting the profiles of the SiII lines λλ5041.024, 5055.984, 5978.930, 6347.109, and 6371.371 Å. Finally, our analysis reveals solar composition of oxygen, magnesium, iron, titanium, and chromium. No helium lines have been detected, then, in agreement with the determined $T_{\rm eff}$, helium abundance has been assumed also solar (Leone & Lanzafame 1998).

An example of spectral synthesis in the range λλ4400–4600 Å is shown in Fig. 3.

5 MASS AND AGE OF THE PRIMARY COMPONENT FROM PROSECCO MODELS

In order to estimate mass and age of the primary component, we applied the Bayesian analysis, a statistical method based on the

[3] IDL (Interactive Data Language) is a registered trademark of Harris Geospatial.

Downloaded from https://academic.oup.com/mnras/article-abstract/477/2/2020/4942279 by guest on 26 February 2020

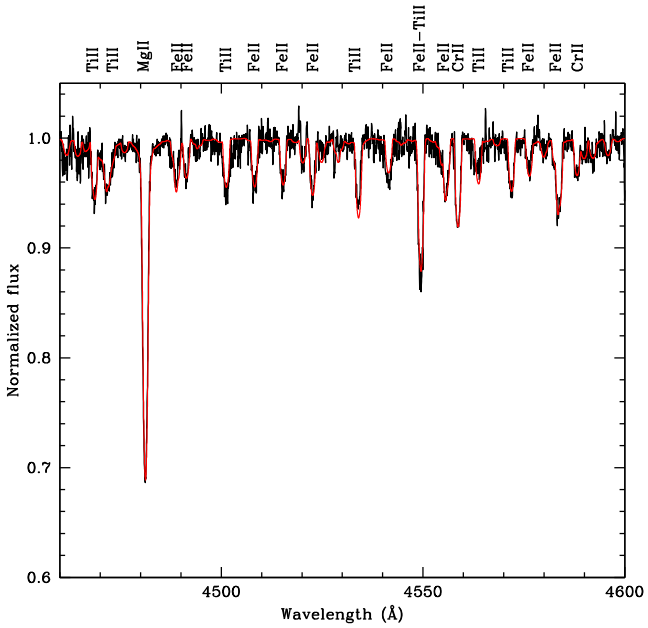

Figure 3. Portion of spectrum for KIC 7599132 with overimposed (red lines) the synthetic spectrum computed with the parameters derived in this study. The chemical abundances for the identified spectral lines are solar.

comparison between observational data and theoretical predictions of evolutionary models. The procedure, already used for pre-main-sequence (PMS) objects (see e.g. Giarrusso et al. 2016; Gennaro, Prada Moroni & Tognelli 2012, hereafter GPT12), has been here developed under the Jørgensen & Lindegren (2005, hereafter JL05) and the GPT12 formalism.

By referring to a single star, let $\boldsymbol{q}$ be the vector of *stellar observational quantities*, that in our case are effective temperature ($T_{\rm eff}$) and surface gravity (g), $\boldsymbol{p}$ the vector of *model parameters*, i.e. age (τ), mass (μ), and initial metallicity (ζ), that include the quantities we want to derive, and $\boldsymbol{\Xi}$ the vector of *meta parameters* whose values identify a class of stellar models, e.g. mixing length ($\alpha_{\rm ML}$), primordial helium abundance ($Y_{\rm P}$), and helium-to-metal enrichment ratio ($\Delta Y/\Delta Z$) . For the Bayes' theorem, the *posterior probability* $f(\boldsymbol{p}|\boldsymbol{q})$ of getting $\boldsymbol{p}$-values given the observed $\boldsymbol{q}$-data results

$$f(\boldsymbol{p}|\boldsymbol{q}) \propto L(\boldsymbol{p}|\boldsymbol{q}) f_{\rm p}(\boldsymbol{p}) \tag{1}$$

where the constant of proportionality is chosen so that $\int f(\boldsymbol{p}|\boldsymbol{q}){\rm d}\boldsymbol{p} = 1$. The *likelihood* $L(\boldsymbol{p}|\boldsymbol{q})$ represents the comparison between observational data and their theoretical predictions from models, while the *prior probability* $f_{\rm p}(\boldsymbol{p})$, i.e. the probability of getting $\boldsymbol{p}$-values independently from $\boldsymbol{q}$ data, allows the introduction of possible available information about model parameters.

By assuming independent Gaussian errors $\sigma_{\rm i}$ for the observed quantities ($i = 1,...,n$ being $n = \dim(\boldsymbol{q})$), the likelihood function is defined as:

$$L(\boldsymbol{p}|\boldsymbol{q}) = \left(\prod_{i=1}^{n} \frac{1}{\sqrt{2\pi}\sigma_{\rm i}}\right) \times \exp\left[-\frac{1}{2}\sum_{i=1}^{n}\left(\frac{q_{\rm i}(\boldsymbol{p}) - q_{\rm i}^{\rm ob}}{\sigma_{\rm i}}\right)^2\right] \tag{2}$$

where $q_{\rm i}^{\rm ob}$ indicates the measured value of the observable $q_{\rm i}$, while $q_i(\boldsymbol{p})$ is the vector of model values for the same quantity.

The most probable value of the quantity we are interested in has been determined through the marginal distribution, obtained by integrating equation (1) over all the model parameters but that we are deriving. The age and the mass are the quantities we want to estimate, while we have assumed that the initial chemical composition is known (Z, see below). So we did not calculate the related marginal distribution, and the known Z-value has been introduced by means of a Gaussian metallicity prior:

$$f_p(\zeta) = \frac{1}{\sqrt{2\pi}\sigma_{\rm Z}} \times \exp\left[-\frac{1}{2}\left(\frac{\zeta - Z}{\sigma_{\rm Z}}\right)^2\right] \tag{3}$$

Thus, the mass marginal distribution $H(\mu)$ and the age marginal distribution $G(\tau)$ we used can be written as follows

$$H(\mu) = \iint L(\tau, \mu, \zeta|\boldsymbol{q}) f_{\rm p}(\zeta) d\tau d\zeta \tag{4}$$

$$G(\tau) = \iint L(\tau, \mu, \zeta|\boldsymbol{q}) f_{\rm p}(\zeta) d\mu d\zeta \tag{5}$$

where we explicitly wrote the vector $\boldsymbol{p}$. We then adopted the mode of $H(\mu)$ and $G(\tau)$ as the Bayesian estimation of the stellar mass (M_1) and age (τ_1), respectively. The confidence interval (CI), i.e. the uncertainty on the derived quantity, was defined as in GPT12 by rejecting the 16 per cent of the total area on each side of the curve.

In our analysis, we adopted as observational data the spectroscopic measurements of effective temperature and surface gravity for the primary star (Section 4).

We computed the necessary grid of stellar evolutionary models by means of the PROSECCO code, described in detail in Tognelli, Prada Moroni & Degl'Innocenti (2015, 2016), with updated outer boundary conditions extracted from the Allard et al. (2011) atmospheres. The $\boldsymbol{\Xi}$-values characterizing the models are $\alpha_{\rm ML} = 2$ (approximated value of the solar calibrated mixing length), $Y_{\rm P} = 0.2485$ (Cyburt 2004), and $\Delta Y/\Delta Z = 2$ (Casagrande et al. 2007). The grid has been obtained for different values of initial chemical composition, namely [Fe/H] from −0.5 to 0.5 dex with a step of 0.05 dex. We converted the initial chemical composition of KIC 7599132 into initial helium Y and metal abundance Z using the relations (Gennaro, Prada Moroni & Degl'Innocenti 2010):

$$Y = Y_{\rm P} + Z\frac{\Delta Y}{\Delta Z} \tag{6}$$

$$Z = \frac{1 - Y_{\rm P}}{1 + \frac{\Delta Y}{\Delta Z} + \frac{1}{(Z/X)_\odot}} \times 10^{-[{\rm Fe/H}]} \tag{7}$$

with the observed [Fe/H] = 0.0 ± 0.1 dex (solar iron content, see Section 4). By adopting the solar-scaled metal distribution $(Z/X)_\odot = 0.0181$ given by Asplund et al. (2009), we derived $Y = 0.274$ and $Z = 0.013$, the latter value representing the a priori information about the initial chemical composition. We adopted a step core overshooting parameter $\beta_{\rm ov} = 0.15$ (Valle et al. 2017) for models with $M > 1.1$ M$_\odot$.

The evolutionary tracks in the grid cover the stellar evolution from the PMS to the end of helium-burning phase for models in the mass range 0.1–10 M$_\odot$ with a mass spacing of 0.005 M$_\odot$. From the models, we built the isochrones with an age spacing 0.01 Myr. Such mass and age sampling have been chosen to get a good resolution when computing the likelihood to clearly identify the most probable value and its CI.

By applying the Bayesian procedure, we obtained $M_1 = 2.4 \pm 0.2$ M$_\odot$ and $\tau_1 = 3.8^{+0.9}_{-0.7}$ Myr. Marginal distributions are plotted in Fig. 4. The radius of the primary we derived from these models is $R_1 = 2.3^{+1.5}_{-0.6}$ R$_\odot$.

6 ANALYSIS OF THE BINARY SYSTEM

To solve the orbit of this binary system and to obtain physical parameters like masses, radii, and luminosities of the primary and

Downloaded from https://academic.oup.com/mnras/article-abstract/477/2/2020/4942279 by guest on 26 February 2020

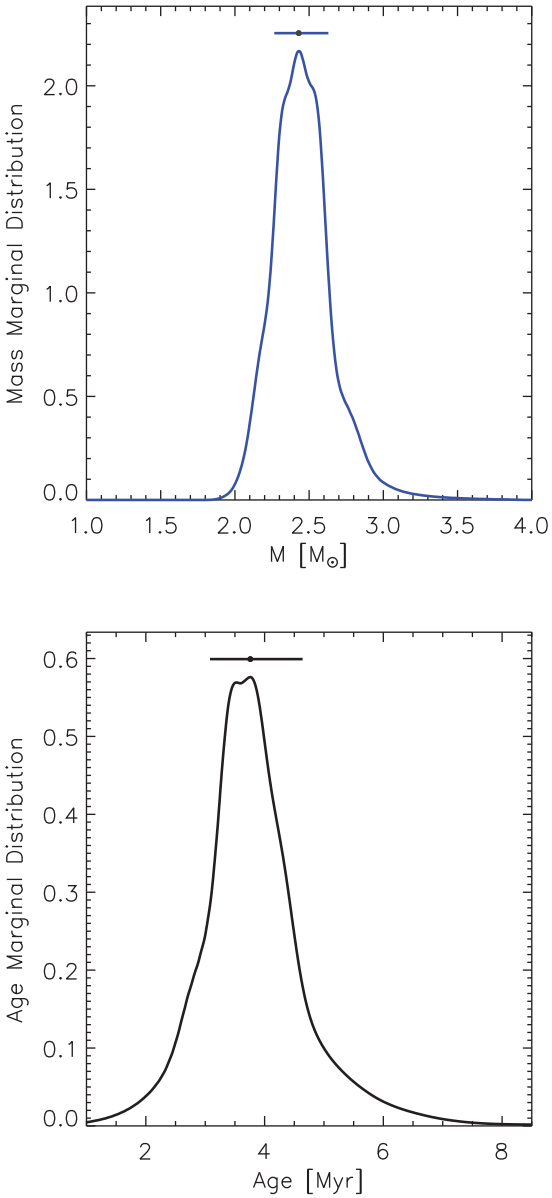

Figure 4. Bayesian results for primary component of KIC 7599132: mass marginal distribution (top panel) and age marginal distribution (bottom panel). Dots indicate the Bayesian estimations, and horizontal solid lines the CIs.

the unseen secondary component, we used the program PHOEBE (version 0.31a), which was developed by Prša and Zwitter (Prša 2003; Prša & Zwitter 2005; Prša et al. 2008). From the observed light and RV curves, PHOEBE estimates physical parameters of the components of a close binary systems that theoretically best matches the data. This code is based on the Wilson–Devinney model (Wilson & Devinney 1971), but it includes also many recent theoretical developments, like extracting individual temperatures from observed colour indices, main-sequence constraining, and proper treatment of the reddening, as well a new graphical user interface (Kallrath & Milone 1999).

To decrease the number of iterations in PHOEBE, we computed an initial solution for this system that we used as a zeroth-order model for the following PHOEBE analysis. The preliminary solution has been derived by analysing *Kepler* LC and spectroscopic velocity curve.

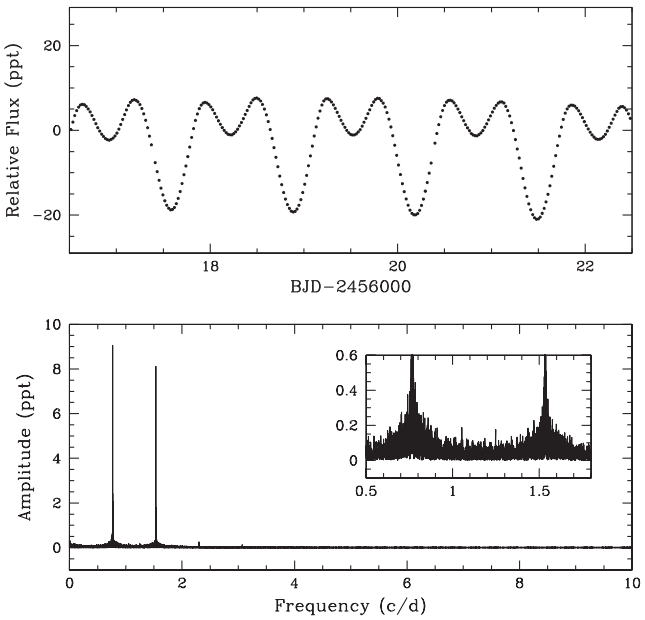

Figure 5. Upper panel: portion of the LC of KIC 7599132 observed by *Kepler*. Bottom panel: periodgram in the interval 0–10 c/d based on the Q0–Q17 data. The insert show the periodogram around the main frequency and the first harmonic (see the text).

6.1 *Kepler* light-curve analysis

Time series photometry of KIC 7599132 used in our analysis were obtained by *Kepler* in long-cadence (30 min exposures) mode, spanning from quarters 0 to 17, comprising 65 859 data points acquired in about 1471 d. The *Kepler* LCs are available as uncorrected simple aperture photometry and with pre-search data conditioning in which instrumental effects are removed (Stumpe et al. 2012; Smith et al. 2012), that we used in our analysis. These data are publicly available on the Barbara A. Mikulski Archive for Space Telescopes (archive.stsci.edu). Upon retrieval, the time sequence was examined and corrected for trends and discontinuities in the LC. To a large extent, this is an automated procedure in which a smooth curve is fitted to the time series and residuals examined for systematic departures indicative of discontinuities. At the same time, points which are clearly outliers are rejected (see Ripepi et al. 2015, for detail). A portion of the LC is shown in the top panel of Fig. 5.

A first visual inspection of the LC clearly shows ellipsoidal variations, characteristic of tidally distorted components of quite different surface brightness. The frequency analysis was carried out with the package PERIOD04 (Lenz & Breger 2005), which is based on classical Fourier analysis techniques and least-squares algorithms. The periodogram of KIC 7599132 is shown in the bottom panel of Fig. 5. The spectrum is dominated by the orbital/rotational frequency at about $f = 0.7671$ c/d and its harmonic $2 \times f$ at $\sim$1.5342 c/d. This is a common feature among ELL (see e.g. Balona 2016). Additional three harmonics can be added to obtain a better least-squares fit of the main frequency, obtaining $f = 0.767082 \pm 0.000002$ c/d with amplitude of 9.05 ± 0.01 ppt (period $P = 1.303642 \pm 0.000003$). Here, the errors have been calculated by using the Monte Carlo option in PERIOD04. The insert in the bottom panel of Fig. 5 shows that the main peaks are surrounded by several side lobes caused by possible phase/amplitude variations. Apart these features, no other significant frequencies are visible in the spectrum till the Nyquist frequency at about 24.4 c/d.

Downloaded from https://academic.oup.com/mnras/article-abstract/477/2/2020/4942279 by guest on 26 February 2020

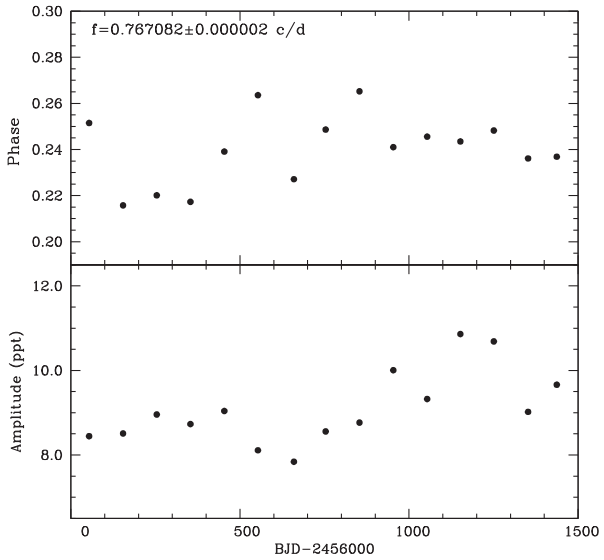

Figure 6. Phase (top panel) and amplitude (bottom panel) variation for the main frequency $f = 0.767082 \pm 0.000002$ c/d KIC 7599132. Filled circles represents the main frequency computed for a chunk of data of 100 d (with the exception of the last one). The sizes of the symbols are approximately of the order of the errors.

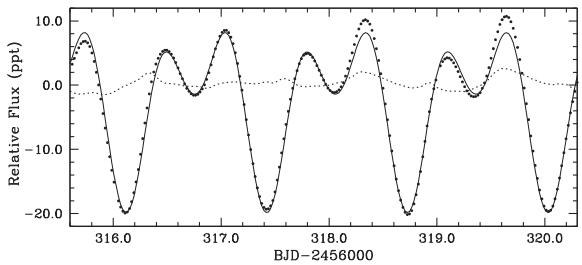

Figure 7. Portion of the LC of KIC 7599132 with overlaid the least-squares fit to the data computer with the fundamental variability frequency $f = 0.767082 \pm 0.000002$ c/d and its first four harmonics (solid line). Dotted line reports the difference between observed and predicted signal (calculated at the JD of the observations).

As we verified that the *Kepler* spectral window of *Kepler* is not able to entirely explain the side lobes around the main variability frequency, we decided to study possible phase/amplitude variations. To this aim, we divided our time series in 15 chunks 100 d each (apart the last one which is 71 d long), and adopted again PERIOD04 by using its 'calculate amplitude/phase variation' function to reach our goal. Note that the size of the chunks were chose to assure a high precision on the frequency (phase) determination, but we checked that the analysis does not really depend on this choice and persist even with smaller chunks of 50 or 20 d. The result of this calculations is displayed in Fig. 6 which shows the phase and amplitude variations for the main variability frequency f=0.767082 ± 0.000002 c/d of KIC 7599132. An inspection of the figure reveal changes in phase of the order of $\sim \pm 0.02$ corresponding to $\sim \pm 0.015$ d and peak-to-peak variations in amplitude of the order of 3 ppt. To verify if these numbers make sense, we visually inspected the LC after overplotting the least-squares fit to the data calculated with the main variability frequency and its first four harmonics. The result of this exercise is shown in Fig. 7, where it is possible to appreciate the oscillation of the best-fitting line around the data. The anticipation/delay of the fit with respect to the data is of the order of 0.013 d, as expected on the basis of the calculated phase variation. Similarly, the variation in amplitude can be directly observed in the figure.

These results explain the presence of the side lobes seen in the frequency spectrum of KIC 7599132. More difficult is the physical interpretation of these variations. Following the works by Balona (2016, 2017) and Balona & Abedigamba (2016), we can ascribe the observed features to the presence of spots passing at different latitudes on the dominant star that is much more luminous of the secondary one, i.e. a hint of differential rotation. In particular, for our target, the overabundance of silicon (≈ 0.5 dex) inferred in Section 4 could be invoked as the possible cause of presence of chemical spots, as discussed in Balona et al. (2015). However, we cannot rule out other explanations for the signal seen as being caused by imperfect detrending or the presence of r modes (Saio et al. 2018), which have been proposed as an alternative mechanism for the signal seen by Balona (2016, 2017) and Balona & Abedigamba (2016). A detailed discussion of these features is however beyond the scope of this work and we remand the interested reader to the discussions in the papers quoted above.

6.2 Initial solution

Following a discussion of Morris (1985) based on the earlier work of Kopal (1959), the LC of an ELL is frequently quasi-sinusoidal and it is commonly represented by the first four terms of a Fourier cosine series of the form:

$$L_1(\phi) = \sum_{n=0}^{3} C_1(n) \cos(n 2\pi\phi + \theta_n) \tag{8}$$

where ϕ is the orbital phase and the subscript 1 refers to the primary component. Equation (8) can be written in the form:

$$L_1(\phi) = A_0 + \sum_{n=1}^{3} C_1(n) \cos(n 2\pi\phi + \theta_n) \tag{9}$$

where $A_0 = C_1(0)\cos\theta_0$ is the brightness of the primary star would have if it were not distorted by the secondary star.

Then, as a first step, we have performed a fit of equation (9) to the data, by using non-linear least-squared fitting procedure MPFIT (Markwardt 2009). We obtained the following values for the coefficients:

$$\begin{aligned} A_0 &: \quad 0.99746 \pm 0.00004 \\ C_1(1) &: \quad 0.00905 \pm 0.00005 \\ C_1(2) &: \quad -0.00811 \pm 0.00005 \\ C_1(3) &: \quad 0.00024 \pm 0.00005 \\ \theta_1 &: \quad 0.977 \pm 0.006 \\ \theta_2 &: \quad 2.285 \pm 0.007 \\ \theta_3 &: \quad 0.5 \pm 0.2 \end{aligned}$$

In particular, as stated in equation (6) of Morris (1985), the amplitude of the $\cos(2\phi)$ term can be expressed via the following equation:

$$\frac{q R_1^3 \sin^2 i}{a^3} = -\frac{3.07 \Delta m (3 - u_1)}{(\tau_1 + 1)(15 + u_1)} \tag{10}$$

where $q\,(= M_2/M_1)$ is the mass ratio between the components, R_1 is the radius of the primary, a is the semimajor axis of the relative orbit (both expressed in solar units). Further, Δm is the amplitude

Downloaded from https://academic.oup.com/mnras/article-abstract/477/2/2020/4942279 by guest on 26 February 2020

Table 2. KIC 7599132 system properties determined from modelling RV and LC by means of PHOEBE.

	Primary		Secondary
JD_0		2457611.347 ± 0.002	
P (d)		1.30364 ± 0.00006	
e		0.03 ± 0.01	
ω		343° ± 7°	
γ (km s^{-1})		− 19 ± 3	
K_1 (km s^{-1})		43 ± 4	
$a_1 \sin i$ ($R_\odot$)		1.1 ± 0.1	
$f(m)$ ($M_\odot$)		0.011 ± 0.003	
a ($R_\odot$)		7.3 ± 0.1	
q		0.30 ± 0.01	
i (°)		35° ± 2°	
$\Omega(L_1)$		2.55 ± 0.02	
$\Omega(L_2)$		2.28 ± 0.02	
F		1.06 ± 0.02	
Albedo	1		0.50 ± 0.02
$T_{\rm eff}$ (K)	10200 ± 150		4000 ± 250
$\log g$	3.9 ± 0.1		3.9 ± 0.2
M ($M_\odot$)	2.4 ± 0.1		0.7 ± 0.1
Ω	2.87 ± 0.02		2.85 ± 0.02
R ($R_\odot$)	3.0 ± 0.2		1.5 ± 0.2
$M_{\rm bol}$	− 0.03 ± 0.07		5.48 ± 0.03
$\log L$ ($L_\odot$)	1.9 ± 0.1		− 0.3 ± 0.2

of the LC given by $\Delta m = 2\,C_1(2)$ and u_1 and τ_1 are the limb- and gravity-darkening coefficients of the primary star, respectively. For the *Kepler* passband filter, these coefficients are taken from Claret & Bloemen (2011): $u_1 = 0.4136$ (linear cosine law) and $\tau_1 = 0.4833$.

By using the velocities reported in Table 1, preliminary orbital elements have been determined by a weighted least-squares fitting of the following equation:

$$V_{\rm rad} = \gamma + K_1[\cos(\theta + \omega) + e\cos\omega] \tag{11}$$

where γ is the RV of the centre of mass, e is the eccentricity of the orbit, ω is the longitude of the periastron, θ is the angular position of the star measured from the centre of mass at a given instant, and K_1 is the semi-amplitude of the velocity curve as given by the formula:

$$K_1 = \frac{2\pi a_1 \sin i}{P\sqrt{1-e^2}} \tag{12}$$

where P is the orbital period of the system, a_1 is the semimajor axis of the primary component, and i is the inclination angle between the orbital plane and the plane of sky. Errors have been estimated as the variation in the parameters which increases the χ^2 of a unit. We obtained the parameters reported in Table 2, where the mass function $f(m)$ is defined as:

$$f(m) = M_1 \frac{q^3 \sin^2 i}{(1+q)^2} \tag{13}$$

As for the eccentricity, we obtained $e = 0.03 \pm 0.05$. Since this small value, we decided to apply the Lucy & Sweeney (1971) criterion to our RVs, reaching the conclusion that an elliptical orbit is significant only at the 5 per cent confidence level and therefore a circular orbit should be assigned to this star. This result has important implications about the system synchronization, in fact, according to the studies by Zahn (1989) and Zahn & Bouchet (1989), the synchronization proceeds much faster than the circularization of the orbit, since the angular momentum of the orbit is larger than that stored in the stars. For such a reason, by using equation (3) of Zahn & Bouchet (1989) we estimated circularization time for our system, which results $t_{\rm circ} \approx 0.65$ Myr, well before the estimated age of our target of $\tau_1 = 3.8^{+0.9}_{-0.7}$ Myr, derived in Section 5. Moreover, the orbital period is in agreement, within the experimental errors, with the photometric period found in Section 6.1. These evidences led us to make the reasonable assumption that the revolution and rotation are synchronized.

With this hypothesis, we can relate the projected rotational velocity to the radius of the primary and period as follows:

$$v_e \sin i = \frac{50.6 R_1 \sin i}{P} \tag{14}$$

where P is the period expressed in days and R_1 is the radius expressed in solar units.

From the *Kepler*'s third law follows:

$$a = 4.207\, P^{2/3}\, M_1^{1/3}\, (1+q)^{1/3} \tag{15}$$

where period is expressed in days, M_1 in solar mass, and a in solar radii.

Thus, if we know mass and projected rotational velocity of the primary component, we can solve iteratively the four equations (10), (13), (14), and (15), for the four unknowns R_1, q, a, and i.

Adopting the mass found in Section 5 for the primary component, the $v_e \sin i$ derived from the fitting of the spectral lines, the mass function obtained from the RV curve, and the period from spectroscopic/photometric observations, we found the following solution:

$$\begin{aligned} R_1 &: \quad 3.1 \pm 0.1 R_\odot \\ q &: \quad 0.30 \pm 0.01 \\ a &: \quad 7.30 \pm 0.02 R_\odot \\ i &: \quad 35° \pm 2° \end{aligned}$$

From this mass ratio and the assumption for M_1, it follows that $M_2 \approx 0.7\ M_\odot$.

6.3 PHOEBE modelling

As input parameters for PHOEBE, we used the effective temperature, surface gravity, and metallicity for the primary component derived in Section 4 and the preliminary orbital solution, as well the values of q, i, a, R_1, and $M_{1,2}$ (reported in Section 6.2).

The type of close binary to be modelled by PHOEBE is selected from a range of options. According to the Roche lobe calculator (Leahy & Leahy 2015), our primary star does not fill its Roche lobe, thus we adopted a detached configuration for the system. We found that this option provided the solution that best fits all the *Kepler* data. Moreover, the option of an atmospheric model for the stars was enabled as was the option of a reflection effect (with no multiple reflections). Factors such as third light, opacity, extinction, and starspots were not considered.

Owing to the radiative nature of A-type stars, the albedo of the primary component was set to one (Claret 2001), while given the unknown nature of the secondary, its albedo was kept as free parameter. The values of gravity- and limb-darkening coefficients for the *Kepler* filter are based on Claret & Bloemen (2011) tables. In particular, for the limb-darkening, we adopted a logarithmic law (see equation 4 of Claret & Bloemen 2011) of the form:

$$\frac{I_{1,2}(\mu)}{I(1)} = 1 - e_{1,2}(1-\mu) - f_{1,2}\mu\ln\mu \tag{16}$$

where $e_{1,2} = 0.5292, 0.7736$ and $f_{1,2} = 0.2733, 0.0031$, and for the gravity-darkening, we adopted $\tau_{1,2} = 0.4833, 0.4703$, where the

Downloaded from https://academic.oup.com/mnras/article-abstract/477/2/2020/4942279 by guest on 26 February 2020

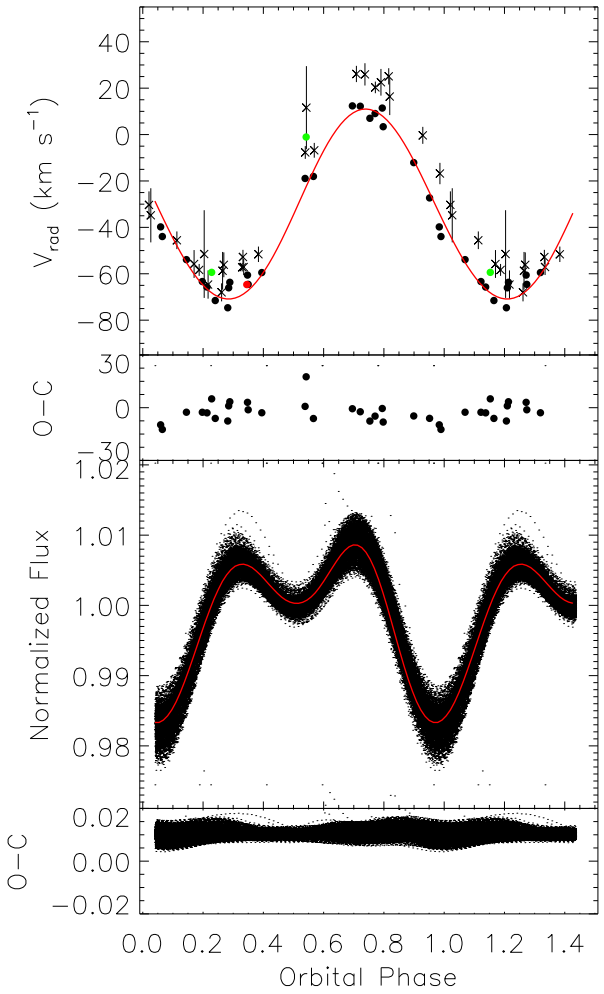

Figure 8. Results of the PHOEBE modelling for KIC 7599132. Upper panel: RV curve, where black dots represent velocities from CAOS, green dots are the velocities from LAMOST, and red dot is the velocity from FRESCO. Bottom panel: folded *Kepler* LC. Residuals are shown below each panel.

indices 1,2 refer to the primary and secondary components, respectively. The passband luminosities for both stars have been calculated by PHOEBE and fixed to HLA = 11.9 and CLA = 0.6.

The minimization routine used was Nelder and Mead's downhill Simplex method Nelder & Mead (1965) that starting from our initial solution reached a convergence in about 10 iterations. RV and LC solutions are overimposed to the observed curves in the top and bottom panels of Fig. 8, respectively.

It is interesting to note that the final solution gave an eccentricity slight different from zero, namely $e = 0.03 \pm 0.01$ and consequently the synchronicity parameter defined as $F = \sqrt{(\frac{1+e}{(1-e)^3})}$ is equal to $F = 1.06 \pm 0.02$. This eccentricity is necessary in order to reproduce the asymmetry between the two maxima in the LC curve. This result is not in contradiction with the hypothesis of synchronicity between orbital and rotational velocities, since at the age of our system the condition of synchronicity is reached before the circularization is complete (Zahn 1989).

The parameters characterizing the system are listed in Table 2.

7 THE PUZZLING SECONDARY STAR

We remark that the properties of the secondary star are weakly constrained by the available photometric and spectroscopic data. In

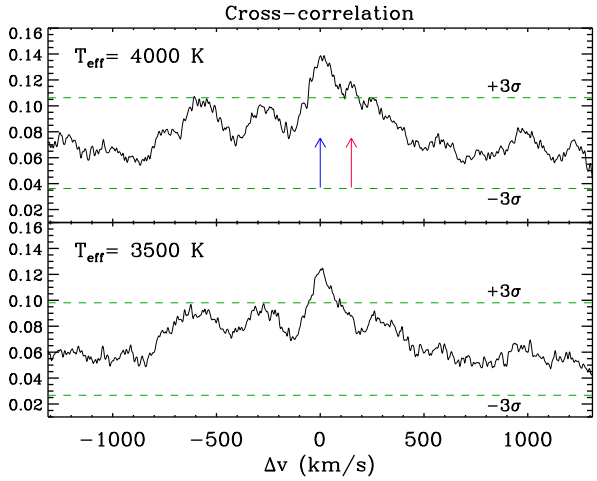

Figure 9. CCFs between simulated composite spectra and RV templates. The spectra of the two components (synthetic ATLAS9 spectra) have been shifted by 150 km s^{-1} and weighted according to the parameters quoted in Table 2. In the upper panel, an effective temperature of 4000 K has been adopted for the secondary component, while in the bottom, it has been fixed to 3500 K. The two vertical arrows mark the RV of the components and the dashed lines delimit the $\pm 3\sigma$ confidence region.

particular, while PHOEBE modelling enabled to constrain radius and mass, for $T_{\rm eff,\,2} \leq 4000$ K no appreciable changes took place in the LC.

In the attempt to better refine the upper limit for $T_{\rm eff,\,2}$, we have simulated the composed spectrum by using synthetic ATLAS9 spectra calculated at the CAOS resolution with the values of $T_{\rm eff}$ and $\log g$ found with PHOEBE. The $v_{\rm e}\sin i$ values used to broaden the synthetic spectra are 60 and 30 km s^{-1} for the primary and secondary components, respectively, as calculated from the radii and orbital/rotational period (assuming synchronous rotation). We considered the wavelength range λλ5000–6400 Å, where the signal of CAOS spectra is the best (S/N ∼ 50 on the average). The synthetic spectra representing the primary and secondary components have been shifted by 150 km s^{-1}, which is the velocity shift that we expect near the quadratures, and have been co-added weighted by the square of the stellar radii. A noise corresponding to S/N=50 was added to them.

We computed the cross-correlation function (CCF) between the above simulated spectrum and a template with the same temperature as the cool component with negligible rotational broadening. The simulation was done with two values of $T_{\rm eff}$ for the secondary star, namely $T_{\rm eff} = 4000$ and 3500 K, and the results are displayed in Fig. 9. The figure readily shows the peak of the primary component in both cases, and the peak corresponding to the secondary component clearly visible (above the 3σ level) only adopting $T_{\rm eff,\,2} = 4000$ K, while it disappears for $T_{\rm eff,\,2} = 3500$ K. As we do not see any hint of a secondary peak in the CCF of the CAOS spectra with the same templates, we argue that the temperature of the cooler component must be $T_{\rm eff,\,2} \leq 4000$ K, if we adopt the radius of 1.5 $R_\odot$ provided by the LC solution.

Positions of both components in the HR diagram, according to PHOEBE results are shown in Fig. 10 together with the Bayesian age interval for primary component. In the same figure, the PROSECCO PMS evolutionary tracks for Bayesian mass of primary and PHOEBE mass of secondary star are also plotted. It is worthy to note that the PHOEBE solution shows a system age corresponding to the lower limit of the Bayesian age CI of the primary, i.e. ∼3 Myr.

Downloaded from https://academic.oup.com/mnras/article-abstract/477/2/2020/4942279 by guest on 26 February 2020

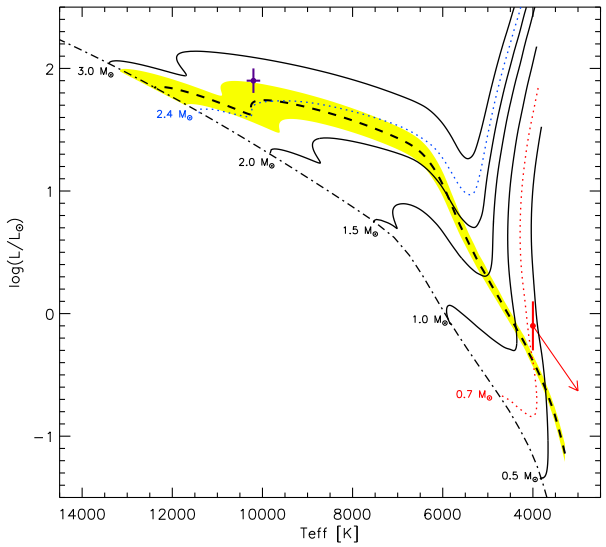

Figure 10. Positions on the HR diagram of primary (violet dot) and secondary (red dot) component of KIC 7599132 according to PHOEBE solution. The values for secondary star are upper limits and the possible trend is highlighted by the arrow. Horizontal and vertical bars indicate temperature and luminosity uncertainties, respectively. Black solid lines show the PROSECCO PMS evolutionary tracks with [Fe/H]=0 up to the ZAMS (dot–dashed line) for the labelled masses. Blue dashed line is the track of the Bayesian mass of primary component, and red dotted line represents the track of the secondary mass obtained with PHOEBE. Yellow area shows the Bayesian age interval for primary component.

8 SUMMARY AND CONCLUSION

In this paper, we have presented a detailed spectroscopic and photometric analysis of the ELL KIC 7599132. Spectroscopic data were taken with CAOS spectropolarimeter installed at the 91 cm telescope of the *Catania Astrophysical Observatory* in 2015 and 2016. Photometric time series were acquired by *Kepler* satellite, quarters 0–17.

Atmospheric parameters for the primary have been derived by comparing synthetic spectra computed with ATLAS9 and SYNTHE with the spectrum obtained by averaging any single spectrum corrected to the velocity of the centre of mass. We obtained the following results: $T_{\rm eff} = 10200 \pm 150$ K and $\log g = 4.1 \pm 0.1$. Spectral lines broadening are compatible with $v_{\rm e} \sin i = 60 \pm 2$ km s^{-1}. Regarding the chemical pattern, we derived a standard chemical composition for helium, oxygen, magnesium, iron, titanium, and chromium, while our analysis revealed an overabundance of silicon (0.5 dex). A determination of mass, 2.4 ± 0.2 M$_\odot$, and age, $3.8^{+0.9}_{-0.7}$ Myr, for the primary have been obtained by Bayesian analysis based on the comparison between observational data and theoretical predictions of evolutionary models.

From each spectrum, by cross-correlation technique, we measured the RVs and derived an orbital motion with a period of 1.30364 ± 0.00006 d. The Fourier analysis of the *Kepler* time series presents a sharp peak at frequency $\nu = 0.7671 \pm 0.0001$ c/d and its harmonics, confirming the previous results by Balona et al. (2015). This frequency corresponds with the orbital period, at least within the experimental errors.

The small value of eccentricity, $e = 0.03$, obtained by fitting our RVs could be neglected on the basis of the Lucy & Sweeney (1971) criterion that we adopted to verify its significance. On the other side, LC modelling shows that this small eccentricity is needed in order to reproduce the slight asymmetry between the two light maxima. This evidence is not in contrast with our initial hypothesis about synchronization. In fact, according to the studies by Zahn (1989), Zahn & Bouchet (1989), and Khaliullin & Khaliullina (2011), the synchronization proceeds much faster than the circularization, since the angular momentum of the orbit is larger than that stored in the stars. Thus, the hypothesis of synchronicity between orbital and rotational motions could be still considered valid, and in particular we estimated circularization time for our system in ≈0.65 Myr, well before the estimated age of our target.

Using available *Kepler* time series and the PHOEBE software package, the data for KIC 7599132 have been fitted with a model of detached binary system. The system properties, determined from iterative modelling, indicate that the masses of the components are $M_1 = 2.4 \pm 0.2$ M$_\odot$ and $M_2 = 0.7 \pm 0.1$ M$_\odot$, the radii are $R_1 = 3.0 \pm 0.2$ R$_\odot$ and $R_2 = 1.5 \pm 0.2$ R$_\odot$, the inclination of the orbital plane with respect the plane of sky is $i = 35^\circ \pm 2^\circ$, and the semimajor axis $a = 7.3 \pm 0.1$ R$_\odot$. From the lack of any spectroscopic evidence, we were able to derive only an upper limit for the effective temperature of the secondary, i.e. $T_{\rm eff,\,2} \leq 4000$ K.

PHOEBE solution together with the Bayesian analysis lead to a system age corresponding to about ∼3 Myr.

ACKNOWLEDGEMENTS

This publication makes use of VOSA, developed under the Spanish Virtual Observatory project supported from the Spanish MICINN through grant AyA2011-24052.

This research has made use of the SIMBAD data base and VizieR catalogue access tool, operated at CDS, Strasbourg, France. This is based on observations made with the CAOS operated by the Catania Astrophysical Observatory.

REFERENCES

Allard F., Homeier D., Freytag B., 2011, in Johns-Krull C., Browning M. K., West A. A., eds., ASP Conf. Ser. Vol. 448, 16th Cambridge Workshop on Cool Stars, Stellar Systems, and the Sun. Astron. Soc. Pac., San Francisco, p. 91

Asplund M., Grevesse N., Sauval A. J., Scott P., 2009, ARA&A, 47, 481

Balona L. A., 2016, MNRAS, 457, 3724

Balona L. A., 2017, MNRAS, 467, 1830

Balona L. A., Abedigamba O. P., 2016, MNRAS, 461, 497

Balona L. A. et al., 2011, MNRAS, 413, 2403

Balona L. A., Catanzaro G. Abedigamba O. P., Ripepi4 V., Smalley B., 2015, MNRAS, 448, 1378

Balona L. A., Baran A. S., Daszyska-Daszkiewicz J., De Cat P., 2015, MNRAS, 451, 1445

Bayo A., Rodrigo C., Barrado Y Navascués D., Solano E., Gutiérrez R., Morales-Calderón M., Allard F., 2008, A&A, 492, 277

Brown T. M., Latham D. W., Everett M. E., Esquerdo G. A., 2011, AJ, 142, 112

Casagrande L., 2007, in Vallenari A., Tantalo R., Portinari L., Moretti A., eds, ASP Conf. Ser. Vol. 374, From Stars to Galaxies: Building the Pieces to Build Up the Universe. Astron. Soc. Pac., San Francisco, p. 71

Castelli F., Hubrig S., 2004, A&A, 425, 263

Castelli F., Gratton R., Kurucz R. L., 1997, A&A, 318, 841 (erratum: 1997, A&A, 324, 432)

Catanzaro G., Leone F., Dall T. H., 2004, A&A, 425, 641

Catanzaro G., Frasca A., Molenda-Zàkowicz J., Marilli E., 2010, A&A, 517, 3

Catanzaro G. et al., 2015, MNRAS, 451, 184

Catanzaro G., Giarrusso M., Leone F., Munari M., Scalia C., Sparacello E., Scuderi S., 2016, MNRAS, 460, 1999

Downloaded from https://academic.oup.com/mnras/article-abstract/477/2/2020/4942279 by guest on 26 February 2020

Claret A., 2001, MNRAS, 327, 989
Claret A., Bloemen S., 2011, A&A, 529, 75
Cyburt R. H., 2004, Phys. Rev. D, 70, 023505
De Cat P. et al., 2015, ApJS, 220, 19
Fitzpatrick E. L., 1999, PASP, 111, 63
Frasca A., Alcalà J. M., Covino E., Catalano S., Marilli E., Paladino R., 2003, A&A, 405, 149
Frasca A., Guillout P., Marilli E., Freire Ferrero R., Biazzo K., Klutsch A., 2006, A&A, 454, 301
Frasca A. et al., 2016, A&A, 594, 39
Gennaro M., Prada Moroni P. G., Degl'Innocenti S., 2010, A&A, 518, A13
Gennaro M., Prada Moroni P. G., Tognelli E., 2012, MNRAS, 420, 986
Giarrusso M. et al., 2016, J. Pharmaceut. Health Care Sci., 703, 012018
Høg E. et al., 2000, A&A, 355, L27
Indebetouw R. et al., 2005, ApJ, 619, 931
Jørgensen B. R., Lindegren L., 2005, A&A, 436, 127
Kallrath J. Milone E. F., 1999, Eclipsing Binary Stars Modelling and Analysis. Springer Verlag, New York
Khaliullin Kh. F., Khaliullina A. I., 2011, MNRAS, 411, 2804
Kopal Z., 1959, Close Contact Binary Systems. John Wiley & Sons, New York
Kurucz R. L., 1993, in Dworetsky M. M., Castelli F., Faraggiana R., eds, ASP Conf. Ser. Vol. 44, IAU Colloq. 138, A New Opacity-sampling Model Atmosphere Program for Arbitrary abundances. Astron. Soc. Pac., San Francisco, p. 87
Kurucz R. L., Avrett E. H., 1981, SAO Special Rep., 391
Kurucz R. L., Bell B., 1995, Kurucz CD-ROM No. 23
Leahy D. A., Leahy J. C., 2015, Comput. Astrophys. Cosmol., 2, 4
Lehmann H. et al., 2011, A&A, 526, A124
Lenz P., Breger M., 2005, Commun. Asteroseismol., 146, 53
Leone F., Lanzafame A. C., 1998, A&A, 330, 306
Leone F. et al., 2016, AJ, 151, 116
Lucy L. B., Sweeney M. A., 1971, AJ, 76, 544
Luo A.-L., Res. Astron. Astrophys. et al., 15, 1095
Markwardt C. B., 2009, in Bohlender D., Dowler P., Durand D. eds, ASP Conf. Ser., Vol. 411, Non-Linear Least Squares Fitting in IDL with MPFIT, Proceedings of Astronomical Data Analysis Software and Systems XVIII, Quebec, Canada. Astron. Soc. Pac., San Francisco, p. 251
McNamara B. J., Jackiewicz J., McKeever J., 2012, AJ, 143, 101
Morris S. L., 1985, ApJ, 295, 143
Nelder J. A., Mead R., 1965, Comput. J., 7, 308
Paunzen E., 2015, A&A, 580, 32
Prša A., 2003, in Munari U., ed., ASP Conf. Ser. Vol. 298, Gaia Spectroscopy: Science and Technology. Astron. Soc. Pac., San Francisco, p. 457
Prša A., Zwitter T., 2005, ApJ, 628, 426
Prša A., Guinan E. F., Devinney E. J., DeGeorge M., Bradstreet D. H., Giammarco J. M., Alcock C. R., Engle S. G., 2008, ApJ, 687, 542
Reinhold T., Gizon L., 2015, A&A, 583, 65
Ripepi V., Balona L., Catanzaro G., Marconi M., Palla F., Giarruso M., 2015, MNRAS, 454, 2606
Saio H., Kurtz D. W., Murphy S. J., Antoci V. L., Lee U., 2018, MNRAS, 474, 2774
Skrutskie M. F. et al., 2006, AJ, 131, 1163
Smith J. C. et al., 2012, PASP, 124, 1000
Stumpe M. C. et al., 2012, PASP, 124, 985
The Hipparcos and Tycho Catalogues, ESA 1997
Tognelli E., Prada Moroni P. G., Degl'Innocenti S., 2015, MNRAS, 449, 3741
Tognelli E., Prada Moroni P. G., Degl'Innocenti S., 2016, MNRAS, 460, 3888
Valle G., Dell'Omodarme M., Prada Moroni P. G., Degl'Innocenti S., 2017, A&A, 600, A41
Wilson R. E., Devinney E. J., 1971, ApJ, 166, 605
Wright E. L. et al., 2010, AJ, 140, 1868
Zahn J.-P., 1989, A&A, 220, 112
Zahn J.-P., Bouchet L., 1989, A&A, 223, 112
Zucker S., Mazeh T., Alexander T., 2007, ApJ, 670, 1326

This paper has been typeset from a TEX/LATEX file prepared by the author.

Downloaded from https://academic.oup.com/mnras/article-abstract/477/2/2020/4942279 by guest on 26 February 2020